Sound & Vibration
DOI:10.32604/sv.2020.010679
Article

Tech Science Press

Frequencies of Lock Gate Structure Coupled with Reservoir Fluid

Priyaranjan Pal*

Motilal Nehru National Institute of Technology Allahabad, Prayagraj, 211004, India
*Corresponding Author: Priyaranjan Pal. Email: prpal2k@gmail.com
Received: 18 March 2020; Accepted: 15 April 2020

Abstract: This study determines the natural frequencies of the lock gate structure, considering the coupled effect of reservoir fluid on one side using the finite element method (FEM). The gate is assumed to be a uniformly thick plate, and its material is isotropic, homogeneous, and elastic. The reservoir fluid is assumed to be inviscid and incompressible in an irrotational flow field. The length of the reservoir domain is truncated using the far boundary condition by adopting the Fourier series expansion theory. Two different assumptions on the free surface, i.e., undisturbed and linearized, are considered in the fluid domain analysis. The computer code is written based on the developed finite element formulations. The natural frequencies of the lock gate are computed when interacting with and without reservoir fluid. Several numerical problems are studied considering the effects of boundary conditions, aspect ratios, and varying dimensions of the gate and the fluid domain. The frequencies of gate reduce significantly due to the presence of fluid. The frequencies increase when the fluid extends to either side of the gate. The frequencies reduce when the depth of the fluid domain above the top edge of the gate increases. The frequencies drop considerably when the free surface condition is taken into account. The results of frequencies of lock gate structure may be useful to the designer if it is experienced in natural catastrophes.

Keywords: Lock gate; reservoir fluid; fluid-structure interaction; frequency; HSDT; FEM

1 Introduction

Fluid-structure interaction problems occur in various structures like storage tanks, dams, offshore structures, piping systems, etc. The lock gate structure is mainly used to regulate the passage of water in the dam-reservoir system. The lock gate structure analysis is quite difficult, while the effect of reservoir fluid is taken into account. When the reservoir system is subjected to any external excitation, an extra force acts on the lock gate structure due to the effect of hydrodynamic pressure. The additional forces generated into the system may damage the structural part of the gate wall. Hence, it is essential to investigate the coupling effects between the lock gate and the reservoir fluid, particularly when the lock gate structure is flexible in type. The motion of the lock gate influences the developed hydrodynamic pressure. At the gate and reservoir fluid interface, the gate's acceleration is transferred to the reservoir fluid, and the hydrodynamic pressure is transferred to the gate. In contact with a fluid, a vibrating

This work is licensed under a Creative Commons Attribution 4.0 International License, which permits unrestricted use, distribution, and reproduction in any medium, provided the original work is properly cited.

structure transfers its vibration to the adjacent fluid and gives rise to fluid motion. This causes an increase in the kinetic energy of the surrounding fluid. Because of increased energy, the natural frequencies of structure and particularly the fundamental frequency decrease significantly compared to the frequencies in a vacuum. The analytical solution of such fluid-structure interaction problems is quite difficult and challenging task. FEM is widely used to solve the coupled fluid-structure interaction problems. A good amount of literature is available on the plate and the fluid problems independently. But, whenever the plate and the fluid interact, the problem becomes difficult, and in such cases, not much literature is available. The above lacuna motivates the author to investigate the lock gate structure in dam-reservoir system to study reservoir's fluid role on the free vibration frequencies of the lock gate.

In the last few decades, fluid-structure interaction problems were investigated by different researchers using various numerical techniques. A few of such relevant literature is presented hereunder, considering the importance of the present problem. Maity et al. [1] presented the hydrodynamic pressure distribution on rigid dams using FEM. The authors modeled the infinite fluid domain by truncating the far boundary considering the classical wave equation. The pressure was assumed as an unknown nodal parameter for compressible fluid. The investigation was limited to two-dimensional analysis only. Zhou et al. [2] studied the free vibration characteristics of a rectangular plate, contact with water on one side. The authors derived the Eigen frequency equations using the Rayleigh-Ritz approach. The effects of depth and width of water, support stiffness, location, and aspect ratio of plate on the Eigen frequencies of plate-water system were investigated. Cheung et al. [3] evaluated the frequencies of a thin plate, connected to a rectangular hole of rigid bottom slab in a liquid-filled rectangular container. The fluid was assumed as incompressible, inviscid and irrotational without taking the effect of surface waves. An analytical-Ritz method was considered to analyze the interaction of the rectangular plate in contact with fluid on one side. Maity et al. [4] studied the coupled effect of elastic structure and fluid using FEM. The domains of the elastic structure and fluid domain were treated as two separate systems (i.e., dam structure and fluid) in the analysis. The governing equation of fluid was expressed in terms of pressure variable, considering the fluid as inviscid and compressible. Teixeira et al. [5] simulated 3D fluid-structure interaction problems using FEM. Authors considered Taylor–Galerkin's scheme and linear tetrahedral elements to analyze the fluid domain. The fluid was assumed as highly or slightly compressible. Maity [6] modeled an infinite reservoir system with an efficient truncation boundary condition, including the radiation effects. Hydrodynamic pressure was evaluated considering the effect of the reservoir's geometry and the adjacent structure. The fluid was assumed as incompressible, inviscid, and irrotational. Pani et al. [7] investigated a lock gate structure in rigid dam, considering the coupled effects of fluid-structure interaction. The authors evaluated the dynamic pressure for both compressible and incompressible fluids. Pani et al. [8] investigated the free vibration characteristics of a rectangular lock gate using FEM, considering the effects of coupled fluid-structure interaction. To discretize the domain, the authors considered four noded plate elements with three degrees of freedom at each node for the lock gate and eight noded brick elements for the fluid domain. The hydrodynamic pressure on a vertical rectangular gate, subjected to ground acceleration, was investigated by Pani et al. [9]. The unknown nodal variables i.e., pressure and displacement, were considered for analysis of fluid domain and gate, respectively. The unbounded reservoir was truncated adjacent to the gate. Pani et al. [10] evaluated the dynamic pressure on a rectangular plate, subjected to a harmonic ground excitation. The authors used the Helmholtz equation for the analysis of fluid domain and Mindlin's theory for the plate. The coupled problem was solved by transferring the plate's acceleration to the fluid and the pressure of the fluid to the plate. Pal [11–14] and Pal et al. [15–16] investigated the coupled frequencies of two-dimensional liquid-filled flexible container considering the effect of sloshing of liquid. Meshless local Petrov-Galerkin (MLPG) method was used to analyze both the liquid and the structural domains. The displacement for the structural wall and pressure for the liquid domain were considered as independent nodal variables. The authors evaluated the

sloshing response in a two-dimensional liquid-filled rigid tank. The MLPG technique was used for the numerical simulation of nonlinear sloshing, and the results were validated with the experimental data. Further authors investigated the sloshing characteristics of liquid in a two-dimensional composite container subjected to external excitation using MLPG technique. Several numerical examples were studied by varying the fiber orientation and aspect ratio of the laminated container wall. Pal et al. [17] studied the free vibration analysis of lock gate structure using first order shear deformation theory (FSDT) for the gate considering the effect of varying fluid domain geometry using truncated far boundary condition. The authors evaluated the natural frequencies of lock gate structure interacting with and without fluid. Singh et al. [18] investigated stiffened lock gate structure frequencies considering the undisturbed liquid free surface using the truncated far boundary condition. The natural frequencies of both bare and stiffened lock gate structures were compared. The aforementioned literature contains little information on the fluid-structure interaction problems. To the best of author's knowledge, it appears that the problem of gate coupled with fluid has not been studied as yet with the importance it deserves.

The present study aims to evaluate the natural frequencies of the lock gate, considering the effects of coupled fluid-structure interaction. A similar study was found in literature where the investigators' used four noded FSDT plate elements with three degrees of freedom at each node to discretize the gate structure and eight noded brick elements for the fluid domain. But, in this study, nine noded HSDT plate elements having seven degrees of freedom at each node for the gate structure and twenty-seven noded hexahedron elements for the fluid domain are considered to acquire more precise results. Further, few studies are available in literature only on the undisturbed free surface of the fluid domain. Here two different conditions are assumed at the fluid's domain top free surface, i.e., undisturbed and linearized free surface. Computer codes are written for the developed methodologies using FORTRAN language to compute the lock gate's natural frequencies. The codes are supplemented with both pre & post-processing modules. At first, the developed code is verified for the problems, already published in the literature, and a good agreement is found. Several numerical problems are solved, and the interesting findings are presented below.

2 Model of Investigation

The mathematical model of a lock gate structure with reservoir fluid used in the present study is shown in Fig. 1b. The model is developed based on an existing lock gate structure model, situated in Texas [19], which is shown in Fig. 1a. It is part of a rigid dam with reservoir fluid on one side. The lock gate is considered to be a vertical rectangular plate of width b_p, height d, and a uniform thickness of t_p connected to an infinitely long rigid dam with the vertical upstream face. The various fluid domain surfaces are labeled in the figure, where h_0 is the depth of reservoir fluid, b is the width of the fluid domain, and L is the truncated length of the fluid domain. At the first stage of analysis, it is assumed that the fluid domain's free surface matches the top edge of the gate, and the sides of the fluid domain match the side edges of the gate (i.e., $h_0 = d$ and $b = b_p$). Hence, the edges of the fluid domain at the interaction interface exactly match the edges of the lock gate. The fluid domain is extruded in a perpendicular plane to that of the gate by developing the truncated far boundary. In the next stage of analysis, the fluid domain extends beyond the lock gate's size, and the investigation is carried out through a parametric variation. The reservoir floor is assumed to be horizontal and rigid.

Two different types of boundary conditions, i.e., simply supported on all edges (SSSS) and clamped on all edges (CCCC), are considered for the lock gate. The gate is assumed to be uniformly thick, and its planar dimensions are varied. Pressure and displacement are taken as unknown nodal variables for the fluid domain and the lock gate, respectively. The top surface of the fluid domain is assumed to be as: (a) undisturbed free

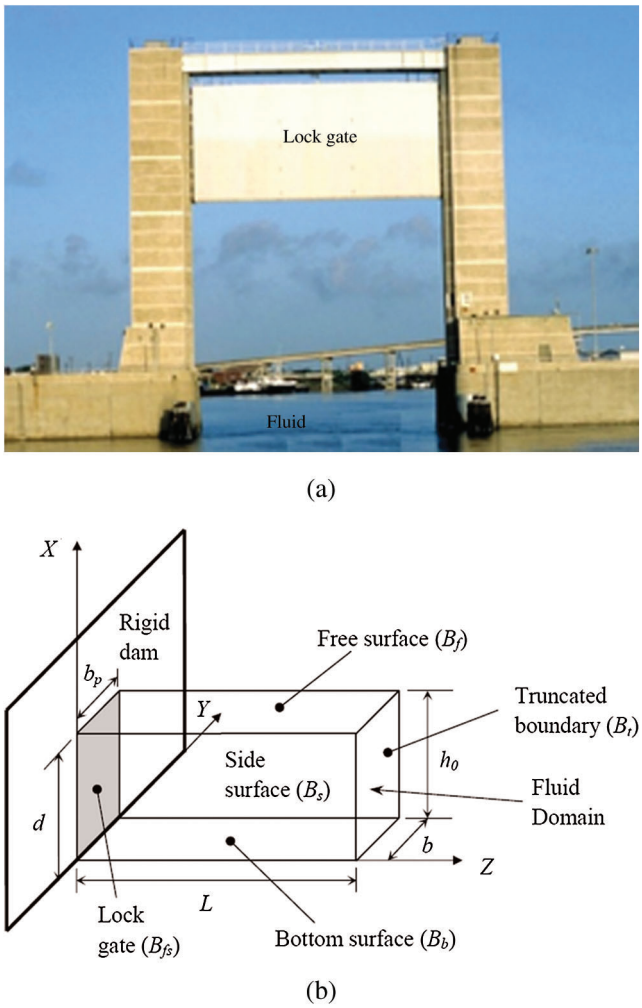

Figure 1: Model for investigation. (a) Existing model [19]. (b) Mathematical model

surface, and (b) linearized free surface. The flow diagram of the analysis is demonstrated in Fig. 2. The mathematical formulations for the lock gate and the fluid domain are presented separately, which is finally coupled with each other. The resulting coupled equation is then used for determining the frequencies of the lock gate structure. Nine noded isoparametric HSDT plate bending elements with seven degrees of freedom at each node for the lock gate and twenty-seven noded isoparametric hexahedron elements with a single degree of freedom at each node for the fluid domain are considered to discretize the domain of system.

3 Governing Equations of the Gate

The displacement components in the plate with respect to the global coordinate system (x-y-z) are assumed as [20–24]

$$\left.\begin{aligned} u(x,y,z) &= u_0(x,y) + z\theta_x(x,y) + z^3\theta_x^*(x,y) \\ v(x,y,z) &= v_0(x,y) + z\theta_y(x,y) + z^3\theta_y^*(x,y) \\ w(x,y,z) &= w_0(x,y) \end{aligned}\right\}, \tag{1}$$

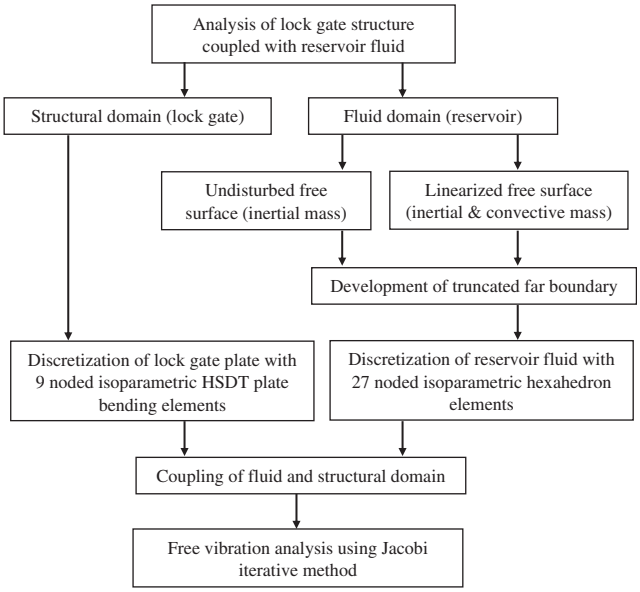

Figure 2: Flow diagram of analysis

where u, v, and w are the displacements in x, y, and z directions, respectively, at any point. At the mid-plane, u_0, v_0 are the membrane displacements and w_0 is the transverse displacement. The parameters θ_x and θ_y are the rotations in the y-z, and x-z planes, respectively. The parameters θ_x^* and θ_y^* are the corresponding higher-order terms. The constitutive equation of an isotropic plate in local coordinate can be written as [24–25]

$$\begin{Bmatrix} \sigma_x \\ \sigma_y \\ \tau_{xy} \\ \tau_{yz} \\ \tau_{xz} \end{Bmatrix} = \begin{bmatrix} Q_{11} & Q_{12} & 0 & 0 & 0 \\ Q_{21} & Q_{22} & 0 & 0 & 0 \\ 0 & 0 & Q_{66} & 0 & 0 \\ 0 & 0 & 0 & Q_{44} & 0 \\ 0 & 0 & 0 & 0 & Q_{55} \end{bmatrix} \begin{Bmatrix} \varepsilon_x \\ \varepsilon_y \\ \gamma_{xy} \\ \gamma_{yz} \\ \gamma_{xz} \end{Bmatrix}, \tag{2}$$

where the material constants are given by

$$Q_{11} = Q_{22} = \frac{E}{(1-\mu^2)}, Q_{12} = Q_{21} = \frac{E\mu}{(1-\mu^2)}, Q_{66} = Q_{44} = Q_{55} = \frac{E}{2(1+\mu)}, \tag{3}$$

where E is the Young modulus, and μ is the Poisson's ratio. The element stiffness matrix is given by [18,21–24]

$$[K^e] = \int_{-1}^{1}\int_{-1}^{1} [B]^T[D][B]|J|d\xi d\eta, \tag{4}$$

where $[B]$ is the strain-displacement matrix obtained by solving the Eq. (1) by differentiating the shape functions of nine-noded isoparametric Lagrangian element for the strain components expressed in Eq. (2). The Jacobian and the material constant matrices have the forms of

$$[J] = \begin{bmatrix} \dfrac{\partial x}{\partial \xi} & \dfrac{\partial y}{\partial \xi} \\ \dfrac{\partial x}{\partial \eta} & \dfrac{\partial y}{\partial \eta} \end{bmatrix}, \tag{5}$$

$$[D] = \begin{bmatrix} A & G & E \\ G & C & F \\ E & F & H \end{bmatrix} \& \left[D^S\right] = \begin{bmatrix} A^S & G^S \\ G^S & C^S \end{bmatrix}, \tag{6}$$

where

$$\left.\begin{array}{l} \left(A_{ij}, G_{ij}, C_{ij}, E_{ij}, F_{ij}, H_{ij}\right) = \int_{-t/2}^{t/2} (1, z, z^2, z^3, z^4, z^6) Q_{ij} dz \quad i,j, = 1,2,6 \\ \&\left(A_{ij}^S, G_{ij}^S, C_{ij}^S\right) = \int_{-t/2}^{t/2} (1, z, z^4) Q_{ij} dz \quad i,j, = 4,5 \end{array}\right\}. \tag{7}$$

The element mass matrix is given by

$$[M^e] = \int_{-1}^{1} \int_{-1}^{1} [N]^T [m][N]|J| d\xi d\eta, \tag{8}$$

where $[N]$ is the shape functions of nine-noded isoparametric Lagrangian element. Here, $[m]$ is defined as follows:

$$[m] = \begin{bmatrix} I_1 & 0 & 0 & I_2 & 0 & \dfrac{c}{3} I_4 & 0 \\ 0 & I_1 & 0 & 0 & I_2 & 0 & \dfrac{c}{3} I_4 \\ 0 & 0 & I_1 & 0 & 0 & 0 & 0 \\ I_2 & 0 & 0 & I_3 & 0 & \dfrac{c}{3} I_5 & 0 \\ 0 & I_2 & 0 & 0 & I_3 & 0 & \dfrac{c}{3} I_5 \\ \dfrac{c}{3} I_4 & 0 & 0 & \dfrac{c}{3} I_5 & 0 & \dfrac{c^2}{9} I_7 & 0 \\ 0 & \dfrac{c}{3} I_4 & 0 & 0 & \dfrac{c}{3} I_5 & 0 & \dfrac{c^2}{9} I_7 \end{bmatrix} \tag{9}$$

with

$$(I_1, I_2, I_3, I_4, I_5, I_7) = \int_{-t/2}^{t/2} \rho\left(1, z, z^2, z^3, z^4, z^6\right) dz \text{ and } c = -\frac{4}{3t^2}. \tag{10}$$

The discretized system of equations of free vibration of the isotropic lock gate can be written as

$$[\mathrm{M}]\left\{\ddot{\bar{\mathrm{X}}}\right\} + [\mathrm{K}]\{\bar{\mathrm{X}}\} = \{0\}, \tag{11}$$

where $[M]$ and $[K]$ are the assembled mass and stiffness matrices. $\left\{\ddot{\bar{X}}\right\}$ and $\{\bar{X}\}$ are the acceleration and displacement vectors, respectively.

4 Governing Equations of the Fluid

4.1 Undisturbed Free Surface

The actual free surface of the fluid domain is nonlinear in nature. When the free surface fluctuation is small compared to the depth of the fluid domain, the free surface may be assumed to be linear. Further, simplification can be made considering the free surface as undisturbed. In another case, the effect of free surface waves can be considered, which may resemble the actual situation. Linear wave theory, given by Airy [26], is used for accounting the free surface waves. This theory holds effective when the depth of fluid is more than the amplitude of the free surface wave. For inviscid, compressible fluid with a small amplitude motion, the dynamic pressure can be written as [1,4,7,9–10]

$$\nabla^2 p(x,y,z,t) = \frac{1}{c^2}\ddot{p}(x,y,z,t), \tag{12}$$

where ∇^2 is the Laplacian operator, *x, y, z* are the coordinates of the point, and *t* is the time. $c = \sqrt{k/\rho_f}$ is the acoustic wave velocity, k is the bulk modulus, and ρ_f is the density of fluid. For inviscid, incompressible, irrotational fluid flow and considering the acoustic wave velocity to be infinite, Eq. (12) can be modified as [6–7,16–18]

$$\nabla^2 p(x,y,z,t) = 0, \tag{13}$$

here p is the dynamic pressure at a point at any instant of time, which can be derived using finite element formulation considering the appropriate time-dependent boundary conditions.

4.1.1 Boundary Conditions

At the fluid-structure interface (B_{fs}), the pressure gradient is generated, and the pressure vanishes at a very far distance away from the lock gate.

$$\frac{\partial p}{\partial n}(x,y,0,t) = -\rho_f a; \quad p(x,y,\infty,t) = 0. \tag{14}$$

There is no change in pressure around the side surfaces (B_s) of the fluid domain due to the gate's negligible displacement, as it vibrates along the rigid dam.

$$\frac{\partial p}{\partial n}(x,0,z,t) = 0; \quad \frac{\partial p}{\partial n}(x,b,z,t) = 0. \tag{15}$$

There is no change in pressure at the bottom surface (B_b) of the fluid domain. Also, there is no surface wave at the top free surface (Bf).

$$\frac{\partial p}{\partial n}(0,y,z,t) = 0; \quad p(h_0,y,z,t) = 0. \tag{16}$$

where h_0 and b are the height and width of the fluid domain, respectively. ρ_f is the mass density of the fluid, and $a(x, y, 0, t)$ is the acceleration of the fluid-gate interface in the direction of n.

4.1.2 Development of Far Boundary

The far boundary of the fluid domain may be considered at a large distance away from the lock gate. The boundary condition at a far truncated boundary may be developed using the Fourier half range cosine series by solving the Eq. (13) which can be represented as [17–18]

$$p = 4h_0\rho_f a \times \sum_{m=0}^{\infty} \frac{(-1)^{(m+1)}}{\lambda_m^2} Cos\lambda_m \left(\frac{y}{h_0}\right) e^{-\left[\lambda_m\left(\frac{z}{h_0}\right)\right]}, \tag{17}$$

where

$$\lambda_m = \frac{(2m-1)\pi}{2}. \tag{18}$$

At the truncated boundary (B_t), the normal gradient of pressure may be represented as follows:

$$\frac{\partial p}{\partial n} = \left(\frac{\partial p}{\partial n}\right)_{z=L} = \frac{-p}{h_0}\zeta_i, \tag{19}$$

where

$$\zeta_i = \frac{\sum_{m=0}^{\infty} \frac{(-1)^{(m+1)}}{\lambda_m^2} Cos\lambda_m \left(\frac{x}{h_0}\right) e^{-\left[\lambda_m\left(\frac{z}{h_0}\right)\right]}}{\sum_{m=0}^{\infty} \frac{(-1)^{(m+1)}}{\lambda_m^3} Cos\lambda_m \left(\frac{x}{h_0}\right) e^{-\left[\lambda_m\left(\frac{z}{h_0}\right)\right]}}. \tag{20}$$

To obtain the effect of the unbounded fluid domain at the truncation part, ζ_i is determined analytically by assuming m to be a large number.

4.1.3 Finite Element Formulation

The pressure at any point inside the fluid domain may be represented as follows:

$$p = \sum_{i=1}^{n} N_i \bar{p}_i, \tag{21}$$

where N_i is shape function, $\bar{p}_i$ is nodal pressure values corresponding to node i, and n is the number of nodes in an element. Using Galerkin's weighted residual approach, Eq. (13) may be represented as follows:

$$\sum \int_{\Omega_e} N^T (\nabla^2 p) d\Omega_e = 0. \tag{22}$$

The weak form of Eq. (22) may be yielded as follows:

$$\sum \int_{\Omega_e} (\nabla N^T . \nabla p) d\Omega_e - \int_{\Gamma_e} N^T \left(\frac{\partial p}{\partial n}\right) d\Gamma_e = 0, \tag{23}$$

where $\sum$ refers to the summation over all the elements, Ω_e for one element, and Γ_e indicates the boundary surface of an element. Further, using the Green's theorem Eq. (23) may be expressed in the concise matrix form as follows:

$$[G]\{\bar{p}\} = \{B\}, \tag{24}$$

in which

$$[G] = \sum \int_{\Omega_e} (\nabla N^T . \nabla N) d\Omega_e, \tag{25}$$

and

$$\{B\} = \sum\nolimits_s \int_{\Gamma_e} N^T \frac{\partial p}{\partial n} d\Gamma_e. \tag{26}$$

However, the boundary term $\{B\}$ may split into the components (Fig. 1) as follows:

$$\{B\} = \{B_f\} + \{B_{fs}\} + \{B_b\} + \{B_s\} + \{B_t\}. \tag{27}$$

At the free surface,

$$\{B_f\} = 0. \tag{28}$$

At the fluid-structure interface,

$$\{B_{fs}\} = -\rho_f [R_{fs}] \{\bar{a}\}, \tag{29}$$

where

$$\{R_{fs}\} = \sum\nolimits_{S_{fs}} \int_{\Gamma_e} N^T N_s d\Gamma_e, \tag{30}$$

where N_s is the shape functions of gate corresponding to the nodes at the fluid-gate interface, and $\{\bar{a}\}$ is the nodal accelerations vector.

At the bottom surface of fluid domain,

$$\{B_b\} = 0. \tag{31}$$

At the two side faces of fluid domain,

$$\{B_s\} = 0. \tag{32}$$

At the truncated boundary,

$$\{B_t\} = -\frac{1}{h_0} [R_{ti}] \{\bar{p}\}, \tag{33}$$

where

$$[R_{ti}] = \sum\nolimits_{S_t} \int_{\Gamma_e} (N^T \zeta_i N) d\Gamma_e. \tag{34}$$

Combining all the boundary conditions in Eq. (27), Eq. (24) may be represented as follows:

$$[G_i] \{\bar{p}\} = -\rho_f [R_{fs}] \{\bar{a}\}, \tag{35}$$

where

$$[G_i] = [G] + \frac{1}{h_0}[R_{ti}]. \tag{36}$$

4.1.4 Coupled Motion of the Gate and the Fluid

Replacing $\{\bar{a}\}$ by $\left\{-\ddot{\bar{X}}\right\}$ in Eq. (36), the resulting equation is as follows:

$$[G_i]\{\bar{p}\} = \rho_f \left[R_{fs}\right]\left\{\ddot{\bar{X}}\right\}. \tag{37}$$

When the effect of dynamic pressure is considered, Eq. (11) may be written as follows:

$$[M]\left\{\ddot{\bar{X}}\right\} + [K]\{\bar{X}\} = \{\overline{f_s}\}, \tag{38}$$

where $\{\overline{f_s}\}$ is the forcing term developed due to fluid pressure at the interface. Since $p = [N]\{\bar{p}\}$ and $\{\overline{f_s}\}$ is yielded as follows:

$$\{\overline{f_s}\} = -\sum\nolimits_{S_{fs}} \int_{\Gamma_e} [N_s]^T p d\Gamma_e = -\left[R_{fs}\right]^T \{\bar{p}\}. \tag{39}$$

Eq. (38) may be rewritten as follows:

$$[M]\left\{\ddot{\bar{X}}\right\} + [K]\{\bar{X}\} + \left[R_{fs}\right]^T \{\bar{p}\} \ = \{0\}. \tag{40}$$

From Eq. (37), the following is obtained

$$\{\bar{p}\} = \rho_f [G_i]^{-1} \left[R_{fs}\right]\left\{\ddot{\bar{X}}\right\}. \tag{41}$$

Substituting $\{\bar{p}\}$ in Eq. (40), the free vibration equation of the coupled problem can be expressed as follows:

$$[\bar{M}]\left\{\ddot{\bar{X}}\right\} + [K]\{\bar{X}\} \ = 0, \tag{42}$$

where

$$[\bar{M}] = [M] + \rho_f \left[R_{fs}\right]^T \left\{\ddot{\bar{X}}\right\} [G_i]^{-1} \left[R_{fs}\right]. \tag{43}$$

4.2 Linearized Free Surface

4.2.1 Boundary Conditions

Except for the boundary conditions at the top surface and at the truncated far boundary, all other boundary conditions adopted here are the same as that of undisturbed free surface condition. At the top surface (B_f), it is assumed that there is a linearized free wave, which is given by Linear wave theory.

$$\frac{\partial p}{\partial n}(h_0, y, z, t) = \frac{-\ddot{p}}{g}. \tag{44}$$

4.2.2 Development of Far Boundary

The far boundary of the fluid domain may be considered at a large distance away from the lock gate structure. The far truncated boundary may be developed using the Fourier half range cosine series by solving Eq. (13) and can be represented as follows:

$$p = \frac{4\rho_f a}{h_0}\sum_{m=0}^{\infty}\frac{Sin(\lambda_m)}{\left(\frac{\lambda_m}{h_0}\right)^2}\left(e^{-\lambda_m\frac{z}{h_0}}\right)Cos\left(\lambda_m\frac{x}{h_0}\right). \tag{45}$$

The pressure gradient at the far truncated boundary may be represented as follows:

$$\frac{\partial p}{\partial n} = \left(\frac{\partial p}{\partial n}\right)_{z=L} = \frac{-p}{h_0}\aleph_i, \tag{46}$$

where

$$\aleph_i = \frac{\sum_{m=0}^{\infty}\frac{Sin(\lambda_m)}{(\lambda_m)^2}\left(e^{-\lambda_m\frac{z}{h_0}}\right)Cos\left(\lambda_m\frac{x}{h_0}\right)}{\sum_{m=0}^{\infty}\frac{Sin(\lambda_m)}{(\lambda_m)^3}\left(e^{-\lambda_m\frac{z}{h_0}}\right)Cos\left(\lambda_m\frac{x}{h_0}\right)}, \tag{47}$$

where x, y, and z refer the axis along the height, side, and length of fluid domain, respectively.

4.2.3 Finite Element Formulation

In the case of linearized free surface wave, the governing equations considered are the same as presented in Eqs. (21)–(27). Here, the components of Eq. (27) remain unchanged except $\{B_f\}$ and $\{B_t\}$. Hence, at the top free surface

$$\{B_f\} = -\sum_{S_f}\left[\int_{\Gamma_e}\dot{}\left(N^T N\right)d\Gamma_e\right]\frac{\{\ddot{p}\}}{g}, \tag{48}$$

and at the truncated boundary,

$$\{B_t\} = -\frac{1}{h_0}[R_{tis}]\{\bar{p}\}, \tag{49}$$

where

$$[R_{tis}] = \sum_{S_t}\int_{\Gamma_e}\dot{}\left(N^T\aleph_i N\right)d\Gamma_e. \tag{50}$$

Combining all the boundary conditions in Eq. (27), Eq. (24) may be represented as follows:

$$[E_i]\{\ddot{p}\} + [G_{is}]\{\bar{p}\} = -\rho_f\left[R_{fs}\right]\{\bar{a}\}, \tag{51}$$

where

$$[E_i] = \frac{1}{g}\sum\nolimits_{S_f}\left[\int_{\Gamma_e}^{\cdot}\left(N^T N\right)d\Gamma_e\right] \text{ and } [G_{is}] = [G] + \frac{1}{h_0}[R_{tis}]. \tag{52}$$

4.2.4 Coupled Motion of the Gate and the Fluid

After replacing $\{\bar{a}\}$ by $\left\{-\ddot{\bar{X}}\right\}$ in Eq. (51), the resulting equation is defined as follows:

$$[E_i]\{\ddot{p}\} + [G_{is}]\{\bar{p}\} = \rho_f\left[R_{fs}\right]\left\{\ddot{\bar{X}}\right\}. \tag{53}$$

Hence, Eq. (11) may be rewritten as follows:

$$[M]\left\{\ddot{\bar{X}}\right\} + [K]\{\bar{X}\} = \{\overline{f_s}\}, \tag{54}$$

where the forcing term $\{\overline{f_s}\}$ is

$$\{\overline{f_s}\} = -\sum_{S_{fs}}\int_{\Gamma_e}^{\cdot}[N_s]^T p d\Gamma_e = -\left[R_{fs}\right]^T\{\bar{p}\}. \tag{55}$$

Substituting the $\{\overline{f_s}\}$ in Eq. (54), the resulting equation is defined as follows:

$$[M]\left\{\ddot{\bar{X}}\right\} + [K]\{\bar{X}\} + \left[R_{fs}\right]^T\{\bar{p}\} = \{0\}, \tag{56}$$

$$\left\{\ddot{\bar{X}}\right\} = -[M]^{-1}\left\{[K]\{\bar{X}\} + \left[R_{fs}\right]^T\{\bar{p}\}\right\}. \tag{57}$$

After rearranging the Eqs. (53)–(57), the symmetric matrices for the coupled system is yielded as follows:

$$\begin{bmatrix}[K] & 0\\ 0 & \dfrac{[E_i]}{\rho_f}\end{bmatrix}\begin{Bmatrix}\left\{\ddot{\bar{X}}\right\}\\ \{\ddot{p}\}\end{Bmatrix} + \begin{bmatrix}[K][M]^{-1}[K] & [K][M]^{-1}\left[R_{fs}\right]^T\\ \left[R_{fs}\right][M]^{-1}[K] & \dfrac{[G_{is}]}{\rho_f} + \left[R_{fs}\right][M]^{-1}\left[R_{fs}\right]^T\end{bmatrix}\begin{Bmatrix}\{\bar{X}\}\\ \{\bar{p}\}\end{Bmatrix} = \begin{Bmatrix}\{0\}\\ \{0\}\end{Bmatrix}. \tag{58}$$

Eq. (58) is the coupled free vibration equation of the gate structure in which the Eigen frequencies are evaluated by using Jacobi's iteration technique. The iteration continues till the convergence up to third decimal place. The evaluated frequencies of the lock gate are presented herein in the non-dimensional form as

$$\Omega^2 = \rho_p t_p \omega^2 b_p^4/D_p, \tag{59}$$

where ρ_p is the mass density of the gate material, ω is the angular frequency of the gate, b_p is the width of the gate, t_p is the thickness of the gate and D_p is the flexural rigidity of the gate material. Here D_p is taken as

$$D_p = Et_p^3/12\left(1-\mu^2\right), \tag{60}$$

where E and μ are the Young modulus and Poisson's ratio of the gate material, respectively.

5 Numerical Examples and Results

In order to verify the applicability of the present model, non-dimensional frequencies of lock gate are evaluated and compared with published results. The gate material is isotropic, having the mass density of 7850 kg/m^3, Young's modulus of 2.0 × 105 N/mm^2, and Poisson's ratio of 0.3. The mass density of the fluid is 1000 kg/m^3. A number of examples are studied to establish the applicability of developed codes to a wide variety of lock gate problems. To check the optimum mesh division, a convergence study is carried out, which is necessitated to minimize the computational error in the evaluated frequencies of the gate. Computational time depends on the hardware configuration of the computer. The results computed here are using a personal computer of Lintel(R) Core (TM) i7-2600 CPU @ 3.4 GHz with 4.00 GB RAM. The number of nodes on the interacting surface of the lock gate is decided, and consequently, the fluid domain is discretized. Another convergence study is also carried out to measure the possible closeness of the truncation boundary from the gate wall. Numerical problems are solved to investigate the effects of varying dimensions of the fluid domain and the lock gate. Frequencies of the lock gate in contact with the reservoir fluid differ considerably from those without fluid. A series of examples are studied herein to demonstrate the precise results and to observe the effects of linearized free surface wave on the natural frequencies of the lock gate, which is scanty in literature.

Example 1. This example is studied to select an optimum mesh division, required to achieve a minimum error in the evaluated frequencies of lock gate without fluid coupling. A square plate of size 1.0 m × 1.0 m and thickness of 0.01 m is taken for the study, and the results are presented in the non-dimensional form. Both eight and nine noded isoparametric plate bending elements with seven degrees of freedom at each node are considered for evaluating the frequencies, and the results of fundamental frequency for different boundary conditions are illustrated in Fig. 3. Keeping the computational time in mind, it is observed that when all the edges are simply supported, results tend to converge at 6 × 6 mesh for 8-noded element and at 4 × 4 mesh for 9-noded element. Similarly, the results tend to converge at 10 × 10 mesh for 8-noded element and at 5 × 5 mesh for 9-noded element when the gate is clamped on all edges. It is clear that the results for 9-noded element converge at lower mesh size for both the boundary conditions. Hence, the 9-noded simple supported gate can be discretized by 4 × 4 mesh and the clamped gate by 5 × 5 mesh. The same mesh division can be adopted for the fluid domain to synchronize the nodes in between the fluid and the gate. Since nine noded element is used to discretize the lock gate structure, the twenty-seven noded

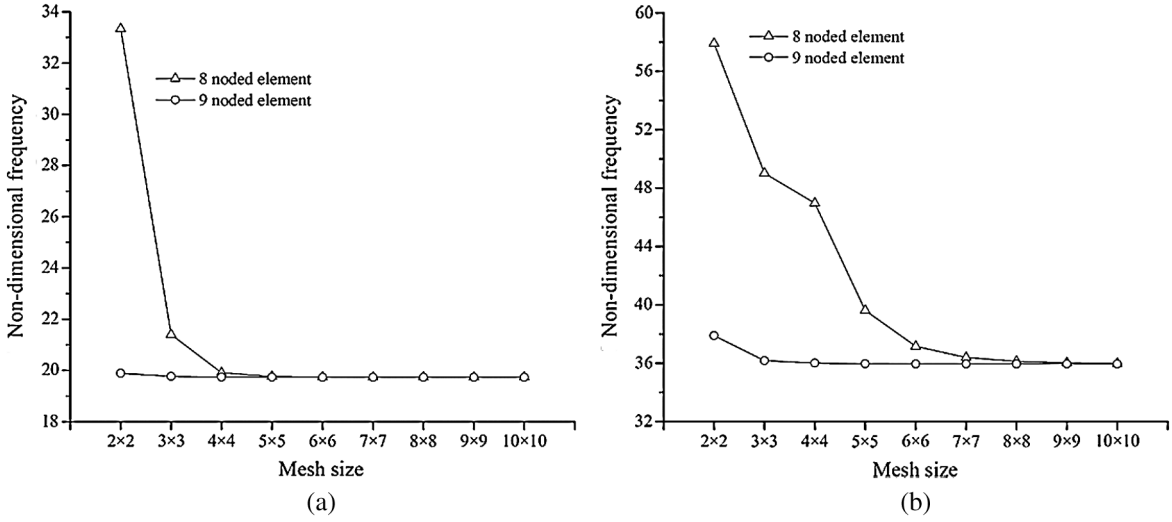

Figure 3: Fundamental frequency of lock gate. (a) Simple supported plate. (b) Clamped plate

hexahedron element can be used to discretize the fluid domain such that the nodes of fluid domain match exactly with the nodes of lock gate at the interface.

Example 2. In this example, the natural frequencies of the lock gate without fluid coupling are evaluated for both the boundary conditions. A square plate of size 1.0 m × 1.0 m and a thickness of 0.01 m is taken for lock gate. A similar problem was solved by Zhou and Cheung [2] using Kirchoff's plate bending theory with a semi-analytical approach; Pani and Bhattacharyya [8] using Mindlin's plate bending theory with finite element approach. Present results are compared with the reported results for the similar type of geometry and boundary conditions except for the element types in FEM. Lock gate frequencies for the first six modes are presented in Tab. 1 and the graphical representations are illustrated in Fig. 4 for the reader's lucidity. One may see that the present results are found to be close proximity to the reported results.

Table 1: Comparison of frequencies of a square lock gate in absence of fluid

Boundary	Investigator	Ω_1	Ω_2	Ω_3	Ω_4	Ω_5	Ω_6
CCCC	Pani et al. [8]	37.496	82.094	82.094	121.402	169.027	169.738
	Zhou et al. [2]	36.007	73.460	73.460	108.370	131.770	132.330
	Present result	35.964	73.832	73.832	108.617	136.180	136.847
SSSS	Pani et al. [8]	20.081	52.590	52.590	84.643	116.216	116.216
	Zhou et al. [2]	19.739	49.348	49.348	78.957	98.696	98.696
	Present result	19.742	49.714	49.714	79.451	103.012	103.012

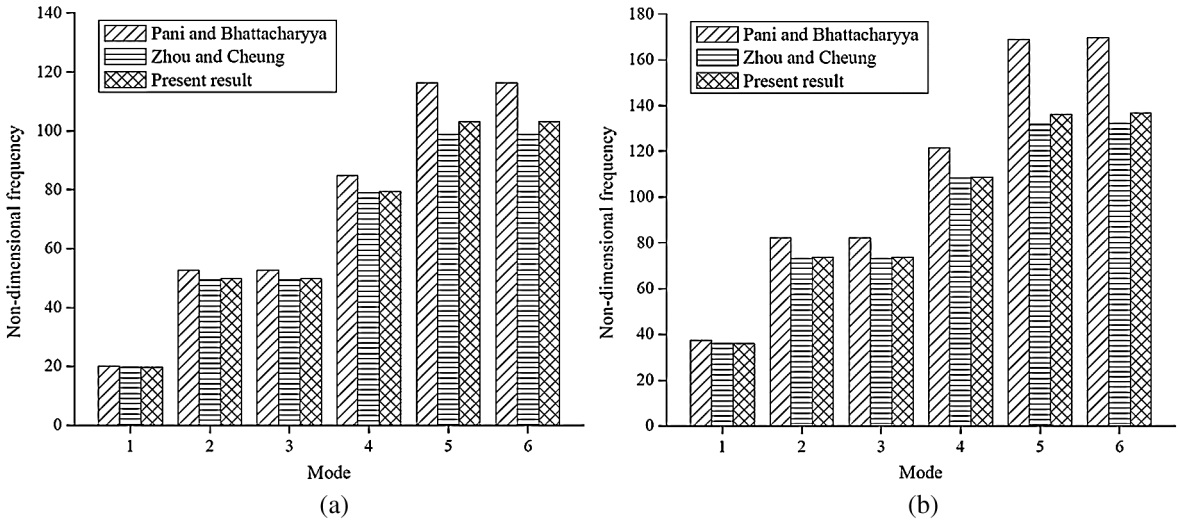

Figure 4: Frequencies of a square lock gate without contact with fluid. (a) Simple supported plate. (b) Clamped plate

Example 3. At the next step, the natural frequencies of the lock gate are evaluated when the gate interacts with the reservoir fluid. The reservoir fluid is assumed to be undisturbed. Lock gate of size 1.0 m × 1.0 m × 0.01 m is used for the investigation. The first six modes of frequencies of lock gate in contact with fluid are presented in Tab. 2. The present results are compared with the reported results, in

Table 2: Comparison of frequencies of a square lock gate in contact with fluid

Boundary	Investigator	Ω_1	Ω_2	Ω_3	Ω_4	Ω_5	Ω_6
CCCC	Pani et al. [8]	25.960	67.072	67.623	104.983	142.936	149.136
	Zhou et al. [2]	25.773	60.981	61.352	94.460	112.83	116.720
	Present result	25.518	62.361	63.528	104.088	130.808	136.978
SSSS	Pani et al. [8]	13.928	43.092	43.569	73.491	100.569	103.382
	Zhou et al. [2]	13.558	39.944	40.381	67.683	84.169	86.493
	Present result	14.365	44.469	45.669	77.783	95.017	97.703

which the geometry and boundary conditions of the problem domain match. Fig. 5 shows the comparison of results for both the boundary conditions of the lock gate when in contact with the fluid. The results shown in figure appear to be very close with that of Zhou et al. [2] and Pani et al. [8], who had solved this problem using the different approaches, as mentioned above. Also, the results are found to be much closer to lower modes of frequency and a little variation for higher modes. These observations certainly validate the present development.

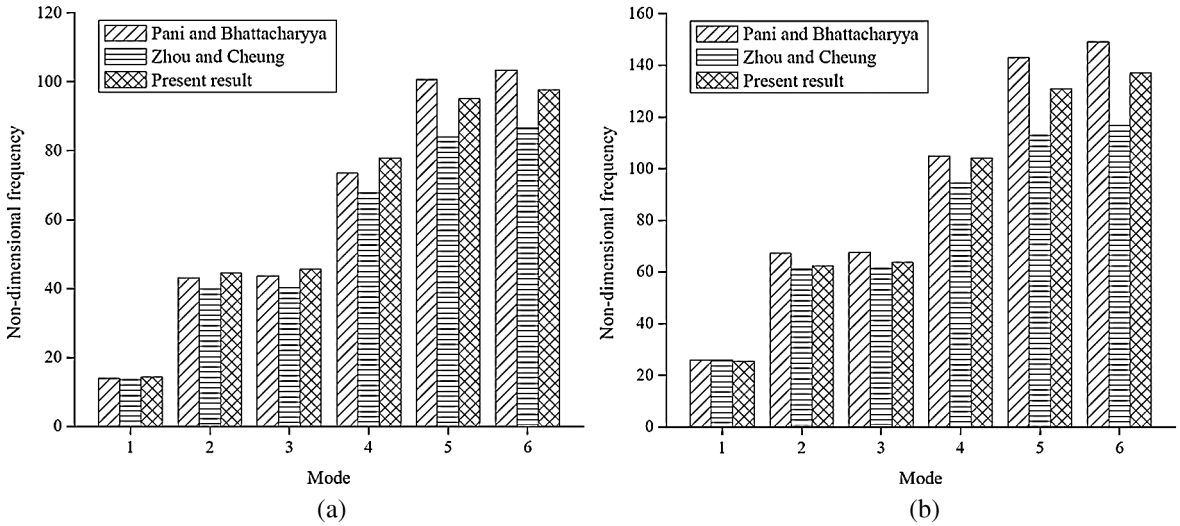

Figure 5: Frequencies of a square lock gate in contact with fluid. (a) Simple supported plate. (b) Clamped plate

Example 4. This example is studied to assess the effectiveness of the far boundary of fluid domain, developed for the possible closeness of the truncation boundary from the lock gate wall. Here a rectangular lock gate is considered to evaluate the natural frequencies of gate for both the boundary conditions. The plate size of 1.5 m width, 1.0 m height, and 0.01 m thick is taken for the investigation. The first six modes of frequencies with varying positions of the truncated boundary are presented in Tabs. 3 and 4 for SSSS and CCCC edges, respectively. The present results are compared with the reported results by Pani et al. [8]. For SSSS edges, the frequencies converge when the far boundary is located at a distance of 1.0 time the height of the lock gate (i.e., the height of the fluid domain). But for CCCC edges, results are about to converge at a distance of 1.5 times the height of the lock gate. Further, in the case of SSSS edges, the results are observed to be on the higher side for lower modes of frequency and are closed for higher modes

Table 3: Frequencies of simply supported lock gate for different positions of the truncated boundary

L/h_0	Investigator	Ω_1	Ω_2	Ω_3	Ω_4	Ω_5	Ω_6
0.25	Pani et al. [8]	9.878	24.708	42.863	48.657	56.466	80.231
	Present result	12.219	26.625	43.358	49.041	55.863	79.815
0.50	Pani et al. [8]	10.997	25.175	43.253	48.941	56.659	80.323
	Present result	13.075	27.281	43.788	49.253	56.120	80.181
0.75	Pani et al. [8]	11.403	25.286	43.281	49.020	56.668	80.327
	Present result	13.080	27.286	43.792	49.254	56.151	80.227
1.0	Pani et al. [8]	11.572	25.328	43.283	49.052	56.668	80.328
	Present result	13.082	27.288	43.793	49.255	56.160	80.241
1.25	Pani et al. [8]	11.627	25.342	43.283	49.063	56.668	80.327
	Present result	13.082	27.288	43.794	49.255	56.164	80.246
1.5	Pani et al. [8]	11.629	25.343	43.283	49.063	56.668	80.327
	Present result	13.082	27.289	43.794	49.255	56.166	80.248

Table 4: Frequencies of clamped lock gate for different positions of the truncated boundary

L/h_0	Investigator	Ω_1	Ω_2	Ω_3	Ω_4	Ω_5	Ω_6
0.25	Pani et al. [8]	20.085	39.018	67.250	68.893	83.123	108.984
	Present result	23.121	40.069	65.780	67.359	79.547	105.051
0.50	Pani et al. [8]	22.072	39.587	67.752	69.384	83.328	109.088
	Present result	23.591	40.476	66.189	67.962	79.961	105.249
0.75	Pani et al. [8]	22.769	39.717	67.921	69.418	83.337	109.094
	Present result	23.590	40.381	66.277	67.942	79.950	105.247
1.0	Pani et al. [8]	23.055	39.765	67.993	69.421	83.338	109.094
	Present result	23.522	40.591	66.791	67.841	79.871	105.242
1.25	Pani et al. [8]	23.148	39.781	68.017	69.421	83.338	109.094
	Present result	23.586	40.270	67.159	67.926	79.939	105.246
1.5	Pani et al. [8]	23.150	39.781	68.017	69.421	83.338	109.094
	Present result	23.636	40.629	67.439	67.993	79.990	105.249

of frequency. However, in the case of CCCC edges, the results are found to be much closer for lower modes of frequency and are in the lower side for higher modes of frequency.

One may say that the developed code produces satisfactory results on different lock gate configurations with varying locations of the truncated boundary. Motivated by the acceptability of present development, established in the aforementioned example problems, some parametric studies are taken up.

Example 5. In particular, this example is studied to observe the variation of lock gate frequencies with varying depth and width of reservoir fluid. The effect on frequencies due to reservoir fluid extends to all sides of gate edges, shown in Fig. 6, is investigated. Where b_s is the equal extent of fluid on both the sides (i.e., left

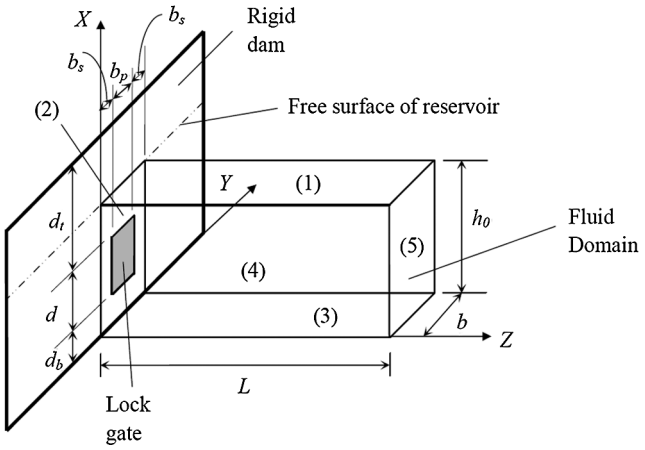

Figure 6: Model of reservoir fluid extending beyond the edges of lock gate

and right) of the lock gate, d_t is the extent of fluid domain above the top, and d_b is the depth of the fluid domain below the base of the lock gate. A square lock gate of size 1.0 m × 1.0 m and a thickness of 0.01 m is taken for both SSSS and CCCC edges. At each depth of fluid (h_0) i.e., 1.0, 1.25, 1.5, 1.75 and 2.0 m, width of fluid (b) is varied as 1.0, 1.5 and 2.0 m and the length of truncated boundary is kept invariable as 1.0 m for SSSS edges. Further, at each depth of fluid (h_0) i.e., 1.0, 1.2, 1.4, 1.6, 1.8 and 2.0 m, width of fluid (b) is varied as 1.0, 1.4 and 1.8 m and the length of truncated boundary is kept invariable as 1.5 m for CCCC edges. The variations of depth and width of the fluid domain for both the edges come naturally as the simply supported gate is discretized by 4 × 4 mesh and the clamped gate by 5 × 5 mesh. Frequencies of the gate for SSSS and CCCC edges are presented in Tabs. 5 and 6, respectively. It is observed that the frequency decreases with the depth of fluid and increases

Table 5: Frequencies of simply supported lock gate with varying fluid depths

h_0	b	Ω_1	Ω_2	Ω_3	Ω_4	Ω_5	Ω_6
1.0	1.0	14.365	44.469	45.669	77.783	96.017	97.703
	1.5	14.430	44.657	46.364	78.070	96.463	97.717
	2.0	14.445	44.698	46.417	78.114	96.693	97.721
1.25	1.0	14.031	43.398	45.383	77.682	95.075	97.688
	1.5	14.181	43.918	46.058	77.995	95.792	97.706
	2.0	14.230	44.068	46.150	78.054	96.171	97.712
1.5	1.0	13.792	42.581	45.332	77.594	94.374	97.676
	1.5	14.014	43.367	45.952	77.930	95.270	97.697
	2.0	14.098	43.644	46.047	78.003	95.764	97.705
1.75	1.0	13.573	41.863	45.315	77.514	93.771	97.667
	1.5	13.862	42.856	45.898	77.871	94.809	97.689
	2.0	13.981	43.252	45.989	77.956	95.398	97.698
2.0	1.0	13.361	41.214	45.308	77.438	93.238	97.658
	1.5	13.714	42.372	45.866	77.815	94.387	97.683
	2.0	13.868	42.875	45.951	77.912	95.059	97.693

Table 6: Frequencies of clamped lock gate with varying fluid depths

h_0	b	Ω_1	Ω_2	Ω_3	Ω_4	Ω_5	Ω_6
1.0	1.0	25.518	63.361	63.528	104.088	130.808	136.978
	1.4	25.548	64.066	63.609	104.129	130.949	136.983
	1.8	25.583	64.256	63.616	104.208	131.055	136.984
1.2	1.0	24.239	61.509	63.455	103.538	130.166	136.973
	1.4	24.520	62.639	63.556	103.832	130.589	136.980
	1.8	24.637	63.048	63.572	103.963	130.759	136.982
1.4	1.0	23.446	60.697	63.423	103.221	129.791	136.970
	1.4	23.911	61.891	63.529	103.585	130.298	136.978
	1.8	24.127	62.421	63.549	103.760	130.522	136.980
1.6	1.0	22.756	60.120	63.402	102.949	129.473	136.968
	1.4	23.392	61.342	63.511	103.368	130.044	136.976
	1.8	23.705	61.946	63.534	103.580	130.311	136.979
1.8	1.0	22.147	59.648	63.386	102.714	129.196	136.967
	1.4	22.913	60.884	63.497	103.174	129.817	136.975
	1.8	23.316	61.543	63.520	103.415	130.118	136.978
2.0	1.0	21.576	59.241	63.374	102.508	128.953	136.965
	1.4	22.462	60.482	63.485	102.999	129.611	136.974
	1.8	22.946	61.185	63.509	103.263	129.941	136.976

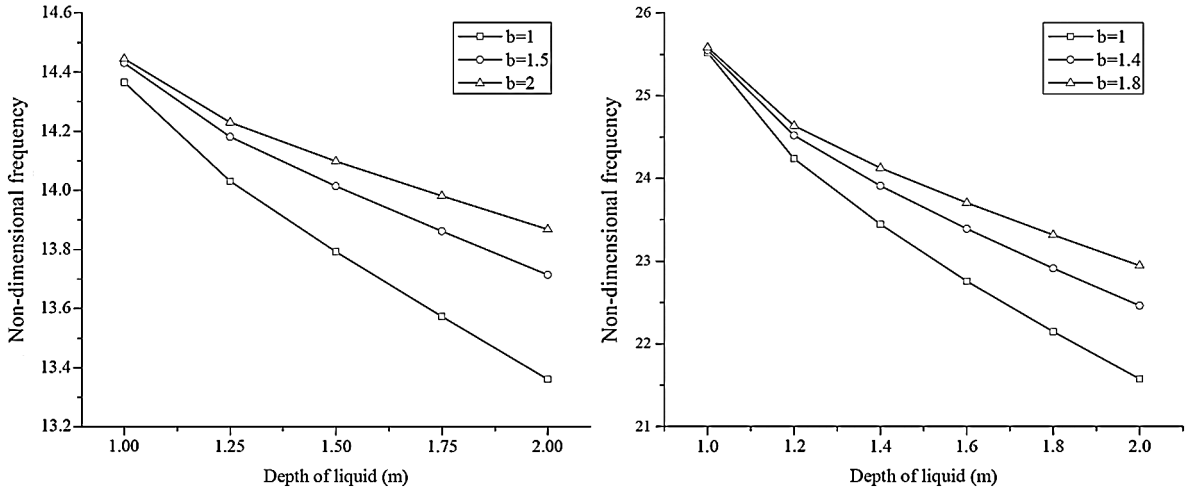

Figure 7: Fundamental frequency of lock gate with varying width and depth of fluid domain. (a) Simple supported plate. (b) Clamped plate

with the width of fluid. This is caused due to the effect of the kinetic energy of the surrounding fluid. These observations are clearly shown in Fig. 7, which illustrates the fundamental frequency of lock gate with varying dimensions of the fluid domain.

Example 6. As the natural step forward, next to the undisturbed free surface condition, the linearized free surface condition is considered for investigation. Frequencies of a square lock gate are evaluated for both the boundary conditions. The size of lock gate is 1.0 m × 1.0 m × 0.01 m. The truncated length of fluid domain is considered to be 1.0 m for the simple supported gate and 1.5 m for the clamped gate. The first six modes of frequencies are demonstrated in Fig. 8 for both SSSS and CCCC edges. It is observed that the frequency of the gate (Fig. 4), falls considerably when the effect of the linearized free surface condition is taken into consideration. This is certainly because of the increase in the surrounding fluid's kinetic energy due to the involvement of convective mass. These values are very low and sensitive to the dam-reservoir system, which may be very critical during the small-magnitude earthquakes. One may see that the variation of the plot is not similar to that of undisturbed free surface condition (Fig. 5).

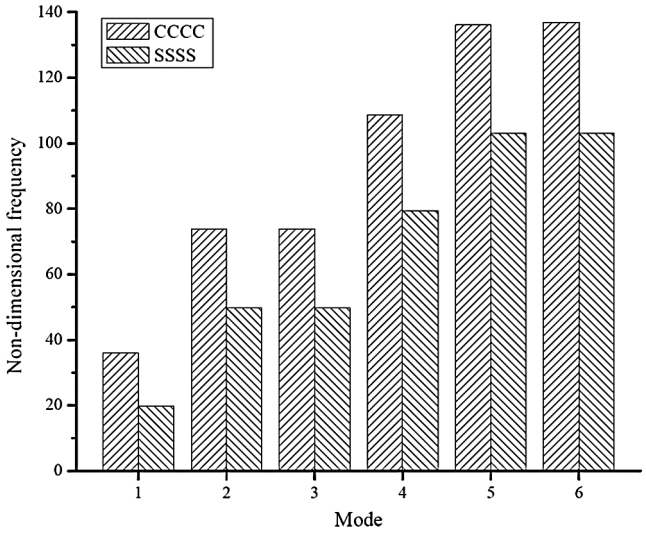

Figure 8: Frequencies of lock gate when interacting with fluid

The fluid may extend beyond the edges of the lock gate during natural disasters. Further, the frequency of lock gate with varying fluid domain dimensions considering the linearized free surface condition is investigated in the following examples.

Example 7. This example is studied to observe the variation of frequencies of the lock gate with varying depth of the fluid domain. Frequencies of the gate are evaluated for both the boundary conditions. A lock gate of size 1.0 m × 1.0 m × 0.01 m is taken for the investigation. The first six modes of frequencies are illustrated in Fig. 9 for SSSS and CCCC edges. It is observed that the frequency decreases with the increase in depth of the fluid domain. It may be caused as the size of the free surface remains the same, and so is the effectuality of the amount of convective mass. The results drop-off for fundamental frequency and converged for higher modes of frequency when the depth of the fluid is increased.

Example 8. Next to the varying depth of fluid, frequencies of the lock gate are evaluated with a varying fluid domain width. The size of the lock gate is 1.0 m × 1.0 m × 0.01 m. The results of the first six modes of frequencies are demonstrated in Fig. 10 for both SSSS and CCCC edges. For undisturbed free surface condition, the frequencies increase with the width of the fluid domain. But for linearized free surface condition, the frequency decreases with the increase in width of the fluid domain, and the frequencies tend to converge when the width of the fluid is increased. It may be because when the width of fluid domain is increased, the size of free surface increases, thereby convective mass.

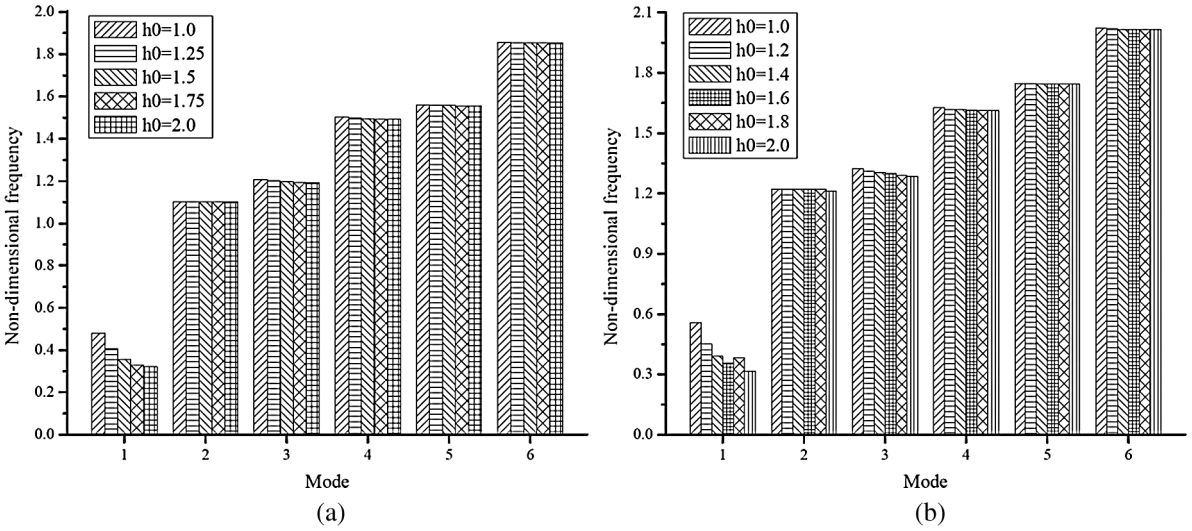

Figure 9: Frequencies of lock gate with varying depth of fluid. (a) Simple supported plate. (b) Clamped plate

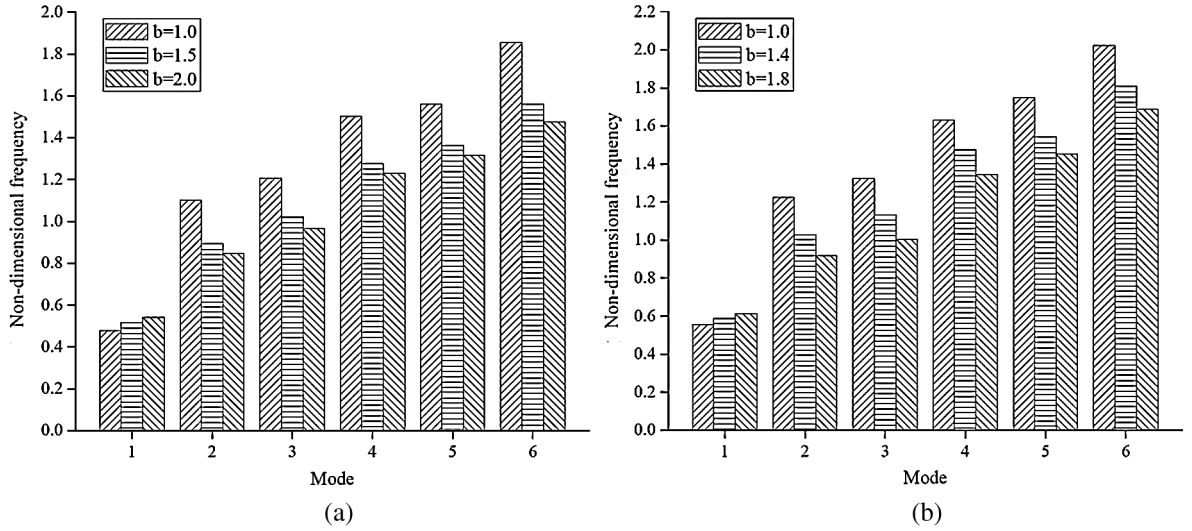

Figure 10: Frequencies of lock gate with varying width of fluid. (a) Simple supported plate. (b) Clamped plate

6 Conclusions

A three-dimensional finite element model was developed based on pressure formulation for the reservoir fluid and displacement for the lock gate structure. This is important since the higher order plate element interacting with the 27-noded hexahedron fluid element. The condition developed at the far boundary of the fluid domain was used efficiently for the numerical truncation of an infinite extent of the fluid domain to a finite one. This concept reduces the computational time to a great extent. The frequencies of the lock gate structure were determined considering the effects of reservoir fluid. Many findings were observed when the gate is interacted with or without the reservoir fluid. The results may be useful to the designers for solving the problem of the lock gate structure. On the basis of the present study, the following conclusions are drawn.

- The frequencies of gate reduce significantly due to fluid presence; when compared in the absence of fluid.
- For simply supported edges, the far boundary is located at a distance of 1.0 time the height of the lock gate, but for clamped edges, it is located at a distance of 1.5 times the height of the lock gate.
- Consideration of the fluid that extends to each side of the gate increases the frequencies of the lock gate and the frequencies gradually remain constant when the extension on each side becomes equal to that of the width of the gate. However, the effect of fluid on each side is significant for lower modes of frequencies, but this effect gradually vanishes for higher modes.
- The effect of fluid below the bottom edge of the gate is significantly less and may be neglected. However, fluid above the top edge affects the lower modes significantly, and insignificantly small for higher modes of frequencies
- When the extent of the fluid domain increases above the gate's top edge, the frequencies reduce and the values appear to be converged when the depth of fluid domain above the top edge exceeds twice the height of the gate.
- The frequencies of the lock gate drop considerably when the linearized free surface condition is taken into account. The variations are significant when compared to the results for undisturbed free surface condition. However, the variation is quite small for the linearized free surface condition because of the convective mass involvement.

Funding Statement: The author(s) received no specific funding for this study.

Conflicts of Interest: The author declares that he has no conflicts of interest to report regarding the present study.

References

1. Maity, D., Bhattacharyya, S. K. (1999). Time-domain analysis of infinite reservoir by finite element method using a novel far-boundary condition. *Finite Elements in Analysis and Design, 32(2),* 85–96. DOI 10.1016/S0168-874X(98)00077-8.
2. Zhou, D., Cheung, Y. K. (2000). Vibration of vertical rectangular plate in contact with water on one side. *Earthquake Engineering and Structural Dynamics, 29(5),* 693–710. DOI 10.1002/(SICI)1096-9845(200005)29:5<693::AID-EQE934>3.0.CO;2-V.
3. Cheung, Y. K., Zhou, D. (2000). Coupled vibratory characteristics of a rectangular container bottom plate. *Journal of Fluids and Structures, 14(3),* 339–357. DOI 10.1006/jfls.1999.0272.
4. Maity, D., Bhattacharyya, S. K. (2003). A parametric study on fluid-structure interaction problems. *Journal of Sound and Vibration, 263(4),* 917–935. DOI 10.1016/S0022-460X(02)01079-9.
5. Teixeira Paulo, R. F., Awruch, A. M. (2005). Numerical simulation of fluid-structure interaction using finite element method. *Computers & Fluids, 34(2),* 249–273. DOI 10.1016/j.compfluid.2004.03.006.
6. Maity, D. (2005). A novel far boundary condition for the finite element analysis of infinite reservoir. *Applied Mathematics and Computation, 170(2),* 1314–1328. DOI 10.1016/j.amc.2005.01.020.
7. Pani, P. K., Bhattacharyya, S. K. (2007). Fluid-structure interaction effects on dynamic pressure of rectangular lock gate. *Finite Elements in Analysis and Design, 43(10),* 739–748. DOI 10.1016/j.finel.2007.03.003.
8. Pani, P. K., Bhattacharyya, S. K. (2008). Free vibration characteristics of a rectangular lock gate structure considering fluid-structure interaction. *Advances in Vibration Engineering, 7(1),* 51–69.
9. Pani, P. K., Bhattacharyya, S. K. (2008). Hydrodynamic pressure on a vertical gate considering fluid-structure interaction. *Finite Elements in Analysis and Design, 44(12–13),* 759–766. DOI 10.1016/j.finel.2008.04.006.
10. Pani, P. K., Bhattacharyya, S. K. (2009). Finite element analysis of a vertical rectangular plate coupled with an unbounded fluid domain on one side using a truncated far boundary. *Journal of Hydrodynamics, 21(2),* 190–200. DOI 10.1016/S1001-6058(08)60136-5.

11. Pal, P. (2009). Sloshing of liquid in partially filled container-an experimentally study. *International Journal on Recent Trends in Engineering, 1(6),* 1–5.
12. Pal, P. (2010). Free-vibration analysis of liquid-filled containers using meshless local Petrov-Galerkin approach. *International Journal on Recent Trends in Engineering, 3(5),* 1–5.
13. Pal, P. (2011). Nonlinear sloshing in rigid containers. *International Journal on Recent Trends in Engineering, 5(3),* 7–11.
14. Pal, P. (2012). Slosh dynamics of liquid-filled rigid containers - a two dimensional meshless local Petrov-Galerkin approach. *Journal of Engineering Mechanics, 138(6),* 567–581. DOI 10.1061/(ASCE)EM.1943-7889.0000367.
15. Pal, P., Bhattacharyya, S. K. (2010). Sloshing in partially filled liquid containers-numerical and experimental study for 2-D problems. *Journal of Sound and Vibration, 329(21),* 4466–4485. DOI 10.1016/j.jsv.2010.05.006.
16. Pal, P., Bhattacharyya, S. K. (2013). Slosh dynamics of liquid-filled composite containers-a two dimensional meshless local Petrov-Galerkin approach. *Journal of Fluids and Structures, 39,* 60–75. DOI 10.1016/j.jfluidstructs.2013.02.002.
17. Pal, P., Singh, R. R., Singh, D. K. (2016). Free vibration frequencies of lock gate structure considering fluid structure interaction. *International Journal of Civil Engineering and Technology, 1(2),* 1–22.
18. Singh, D. K., Duggal, S. K., Pal, P. (2018). Free vibration analysis of stiffened lock gate structure coupled with fluid. *Journal of Structural Engineering, 45(1),* 1–9.
19. Burke, R. (1998). https://www.ruthburkeart.photoshelter.com/image/I0000ghPZWsRsEZU.
20. Reddy, J. N. (1984). A simple higher-order theory for laminated composite plates. *Journal of Applied Mechanics, 51(4),* 745–752. DOI 10.1115/1.3167719.
21. Kant, T., Pandya, B. N. (1988). A simple finite element formulation of a higher-order theory for unsymmetrically laminated composite plates. *Composite Structures, 9(3),* 215–246. DOI 10.1016/0263-8223(88)90015-3.
22. Kant, T., Kommineni, J. R. (1992). C0 finite element geometrically non-linear analysis of fibre reinforced composite and sandwich laminates based on a higher-order theory. *Computers & Structures, 45(3),* 511–520. DOI 10.1016/0045-7949(92)90436-4.
23. Thai, C. H., Train, L. V., Train, D. T., Thoi, T. N., Xuan, H. N. (2012). Analysis of laminated composite plates using higher-order shear deformation plate theory and node-based smoothed discrete shear gap method. *Applied Mathematical Modelling, 36(11),* 5657–5677. DOI 10.1016/j.apm.2012.01.003.
24. Pal, P. (2018). The displacement view of a multilayered HSDT plate. *Journal of Polymer Science and Engineering, 1(2),* 1–8. DOI 10.24294/jpse.v1i2.863.
25. Serdoun, S. M. N., Hamza-Cherif, S. M. (2014). Free vibration analysis of isotropic plates by alternative hierarchical finite element method based on Reddy's C1 HSDT. *American Scientific Research Journal for Engineering, Technology, and Sciences, 9(1),* 1–19.
26. Airy, G. B. (1845). Tides and waves. *Encyclopaedia Metropolitana, 5,* 241–392.